Development of a Computational Model to Aid Prediction of Neurosurgical Brain Shift

N.J. Bennion, M. Potts, A.D. Marshall, S. Anderson and S.L. Evans

Abstract Stereotactic procedures are an increasingly common tool for the diagnosis and treatment of neurological disorders. Common surgeries reliant on a stereotactic reference frame include Deep Brain Stimulation, Stereoelectroencephalography, Stereobiopsy, and high precision intraparenchymal drug delivery. Introduction: Stereotactic neurosurgical procedures are planned and carried out per preoperative medical images in a fixed reference frame. Loss of cerebrospinal fluid and a variety of other factors lead to a displacement of the anatomical target from the stereotactic coordinates, known as brain shift. Aims: To develop a computational model to aid in the understanding and prediction of gravity induced brain shift based on patient repositioning. Methods: The MNI ICBM152 Average Brain Stereotaxic Registration Model was manually segmented and meshed in the Simpleware Scan IP software package. Using FEBio, suitable constitutive models were applied to each region. The model was then loaded to simulate supine-to-prone repositioning. Results: Displacement reached a maximum of approximately 2.4mm, with cortical displacement being concentrated in anterior regions. Conclusions: With good initial results, the future applications of this method appear promising.

This research is funded by the EPSRC and Renishaw Plc. as part of an iCase Studentship. The authors acknowledge the contributions of Rob Harrison, Renishaw Plc.

N.J. Bennion (✉) · M. Potts · A.D. Marshall · S.L. Evans
School of Engineering, Cardiff University, Cardiff CF24 3AA, UK
e-mail: bennionn@cardiff.ac.uk

S. Anderson
School of Engineering, Renishaw Plc, New Mills, Wotton-under-Edge, Gloucestershire GL12 8JR, UK

A. Gefen and D. Weihs (eds.), *Computer Methods in Biomechanics and Biomedical Engineering*, Lecture Notes in Bioengineering,
DOI 10.1007/978-3-319-59764-5_21

Introduction

Stereotactic procedures are an increasingly common tool for the diagnosis and treatment of neurological disorders. Common surgeries reliant on a stereotactic reference frame include Deep Brain Stimulation (DBS), Stereoelectroencephalography, Stereobiopsy and high precision intra-parenchymal drug delivery (Elias et al. 2007; Lewis et al. 2016; Jackson et al. 2001). DBS is used to treat the symptoms of movement disorders such as Parkinson's disease, dystonia, and essential tremors (Hamze et al. 2015). As its name suggests, an electrode is inserted through the skull into a specific region of the deep brain. The surgeon will decide the best regions to aim for based on the condition that requires treatment and any patient specific variation. The subthalamic nucleus (STN), globus pallidus internus (GPi), ventral intermediate thalamus (VIM), and pedunculopontine nucleus (PPN) are common in DBS procedures (Kalia et al. 2013). Given the very small size of these structures, the efficacy of this treatment depends on sub-millimetre accuracy of electrode placement.

Surgeons use pre-operative patient images to identify the electrode trajectory and insertion depth required to reach anatomical targets. It has, however, been long understood that the process of inserting an electrode into the brain leads to a non-rigid deformation known as brain shift (Elias et al. 2007). The existence of brain shift in procedures requiring such accuracy has led to the development of various techniques such as microelectrode recording and intraoperative MRI to account for this phenomenon and to ensure adequate placement of electrodes. Although effective, these additional compensatory measures add time and complexity to the operation (Amirnovin et al. 2006; Ivan et al. 2014).

It has been clearly demonstrated that losing large amounts of cerebrospinal fluid (CSF) can lead to large deformations of both the cortical surface and deep brain (Elias et al. 2007). However, even when surgical protocols developed specifically to limit CSF loss are in place, deep brain displacement of a surgically significant scale is still observed. It is therefore reasonable to conclude that brain shift is not simply a function of CSF loss. As such, a wide range of patient specific factors must be important. Although studies have attempted to assess the impact of some measurable forms of intra-patient variations, such as cerebral atrophy (Azmi et al. 2011), a definitive understanding has not yet been achieved.

In order to develop a method of accounting for brain shift on a patient specific basis, a better understanding of brain shift which occurs with no surgical intervention is required. This is known as anatomical brain shift and occurs in everyone simply with repositioning of the head with respect to gravity. Anatomical brain shift has been studied by MR imaging of patients lying in prone, supine and lateral positions (Hill et al. 1998; Schnaudigel et al. 2010; Monea et al. 2012). Results from such studies have again highlighted that clinically significant displacement of both the deep brain and cortical surface can be expected even with no surgical intervention.

The purpose of this study is to develop a detailed computational model to predict anatomical brain shift. This model can then be used to further our understanding of patient specific geometric and tissue property variation, and its impact on brain shift.

Materials and Methods

Image Segmentation and Model Geometry

Image segmentation was performed manually using Simpleware ScanIP (Synopsys, Mountain View, USA). In order to avoid patient specific anatomical variation the MNI ICBM152 Average Brain Stereotaxic Registration Model (McConnell Brain Imaging Centre, Montreal Neurological Institute, McGill University) was used.

Throughout the early stages of development, models were segmented with increasing levels of anatomic detail. In particular, simplified models suggested that the pia-arachnoid complex (PAC) and dural septa offered considerable support to the brain. This highlighted the need to balance such detail with that for a computationally stable mesh. As a result, the model was segmented into the following parts: skull, brain, ventricular system, pia-arachnoid complex, dural septa, and major sinuses.

The skull was included only to act as an outer limit and was assumed to be rigid in the final model. To improve computational stability some smoothing and manual inclusion/removal of certain areas was also required. Offering important structural support, the tentorium cerebelli and falx cerebri were segmented together with the sinuses adjacent to them. Whether it is correct to assume these structures do not deform significantly will be tested in the future. In this model, the dura mater was assumed to be rigidly attached to the skull and therefore did not play a structural role. The PAC, which surrounds the brain, was segmented as one layer, but split into left, right and inferior sections.

Material Parameters

The segmented geometry was imported into FEBio (Maas et al. 2012) for finite element analysis. Table 1 outlines the FEBio material parameters that were chosen for each region.

Table 1 Material parameters used in the final computational model

Structure	Material model	Material parameters	Elements
Brain	Mooney–Rivlin	$c1 = 0.28$, $c2 = 333$ (Mihai et al. 2015), $k = 1{,}000{,}000$ Pa, $\rho = 1040$ kg/m^3 (Cala et al. 1981)	766,611
PAC	Transversely isotropic Mooney–Rivlin	$c1 = 10$, $c2 = 10$, $c3 = 1.8$, $c4 = 175$, $c5 = 80{,}000$ Pa, lam_max = 1.01 $k = 10{,}000$ Pa (Jin et al. 2006; Jin et al. 2007; Jin et al. 2014; Jin et al. 2011), $\rho = 1007$ kg/m^3 (Levin et al. 1981)	645,023
Ventricles	Isotropic elastic	$E = 1000$ Pa, $v = 0.49$	28,843
Dural septa	Isotropic elastic	$E = 30{,}000{,}000$ Pa (van Noort et al. 1981), $v = 0.49$	158,442

As noted above, the PAC regions were intended to be fiber stiffened in the out of plane vector in order to replicate the tethering action of the arachnoid trabeculae. To achieve this, the PAC structure was split into three regions, with a spherical fiber center assigned to the central point of each hemisphere and the cerebellum. A linear tetrahedral mesh was also generated and refined in Simpleware ScanIP.

Loading

It is not possible to image the brain in an unloaded state as it is always subject to the force of gravity in the initial imaging position. As a result, the model must account for the force difference between the prone and supine positions as opposed to those generated in either position alone. Given that this is a quasi-static analysis with no surgical interventions, the only two loads on the system are gravity and buoyancy force generated by the density difference between brain tissue and CSF. This buoyancy force can be implemented as a pressure on the outside surface of the brain.

The positional change means that the gravitational body load acting is 18.62 m/s^2.

Taking the initial supine imaging position, the pressure P at any point is equal to:

$$P = \rho g h,$$

where ρ is density, g is the gravitational constant and h is the distance parallel to the gravitational field from the top of the fluid body to the point. Taking the anterior limit of the intracranial volume to be h_0 and the posterior limit to be h_1, the pressure distribution at any point in the supine position P_s is:

$$P_s = \rho g(h_0 - h_i),$$

where h_i is the position of the point in the gravitational axis. Similarly, the pressure distribution in the prone position P_p is given by:

$$P_p = \rho g(h_i - h_1)$$

As such, the pressure difference ΔP at any point when moving from supine to prone is

$$\Delta P = P_p - P_s$$

$$\Delta P = \rho g(h_i - h_1) - \rho g(h_0 - h_i)$$

$$\Delta P = -\rho g(h_1 + h_o - 2h_i)$$

This pressure was calculated and applied to every element surface making up the exterior of the brain.

Results

The results of the computational model are shown in Fig. 1. Deformation was concentrated around the corpus callosum and anterior portions of the lateral and third ventricles. In this region the total displacement reached a maximum of 2.36 mm and was mainly a result of component vectors in the gravitational axis.

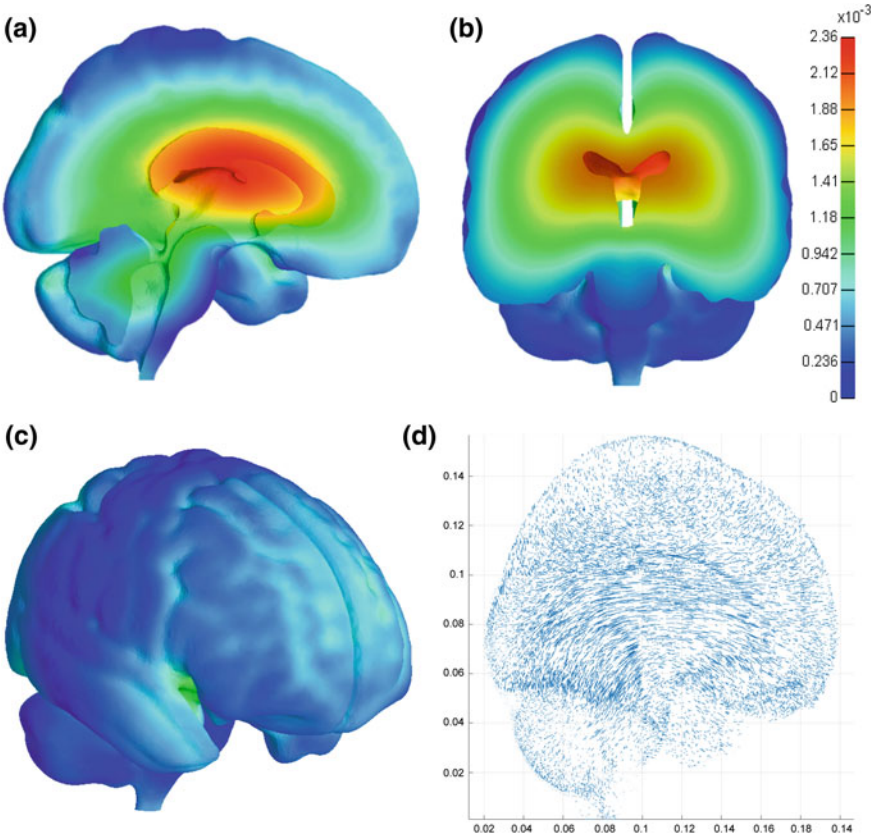

Fig. 1 Scalar deformation in meters that was predicted as a result of supine to prone repositioning (**a**) in a midline section in the sagittal plane, **b** in a coronal section and, **c** on the cortical surface. **d** Is a vector plot visualizing 1/20 of the nodal vectors from the brain and other structures

Cortical displacement was greater in anterior portions of the brain, remaining less than 1 mm in all regions.

Discussion

Although many groups have attempted to model brain deformation for cases where large scale resection of tissue is required, far fewer have investigated predictions for stereotactic cases. Bilger et al. (2011, 2014a, b) also accepted that prediction of CSF loss was impossible. Instead, the authors employed worse case boundary conditions to generate a risk volume that must be avoided to ensure safe insertion of the electrode. This and subsequent related works looked at automation of this process and intra-operative registration of the computational model to a deformed image. These models use a physics-based approach incorporating similar boundary conditions. However, the slight difference in application means comparison of the models directly is not meaningful.

Compared to the study of intraoperative brain shift, little is known about non-rigid brain-skull deformation due to positional effects alone. Early investigations found anatomical brain shift to be less than 1 mm, although this was in the same order of magnitude as the measurement error in the systems available at the time (Hill et al. 1998). More recently, Schnaudigel et al. (2010) found that brain shift was at a maximum in central structures, with a magnitude of 0.6–1.3 mm across their study for supine to prone repositioning. Although taking place relatively quickly, it was also shown that the brain had not settled by 12 min in the scanning position; a consideration which is to be investigated further in the future. In contrast, Monea et al. (2012) found the greatest deformations to be on the cortical surface with a maximum of 7.86 mm for the same prone to supine repositioning. The source of the difference between these two studies is unclear.

The level of deformation found in this study fell very much in line with the results of Schnaudigel et al. (2010). Cortical displacement was limited, but more significant in the anterior half of the brain. The absolute magnitude of displacement was not in the region of those reported by Monea et al. (2012), although distribution was similar. The results of this model suggest a tethering effect of the PAC in tension. The compressive stiffness of the PAC in vivo is not known. It is likely comprised of a slight contribution from the arachnoid trabeculae in buckling, but mainly from redistribution of the CSF when under increased pressure. As the current model does not include any computational fluid dynamics, this aspect has been simplified to standard solid elements with low compressive stiffness and a less-than-incompressible bulk modulus. Finding precise values for these parameters that are required to provide an accurate representation of this redistribution requires further investigation.

Due to a lack of a consensus and large degrees of intra-patient variation seen in the literature, more rigorous validation of this model is not currently possible. Regardless of this, the current study has shown that the combination of detailed

geometry and structure specific material parameterization can offer new insights into the mechanics of anatomical brain deformation. With continued development, this approach has the potential to offer significant improvements to surgical planning.

References

Amirnovin R, Williams ZM, Cosgrove GR, Eskandar EN (2006) Experience with microelectrode guided subthalamic nucleus deep brain stimulation. Neurosurgery. 58(1 Suppl):ONS96–ONS102 discussion ONS96

Azmi H, Machado A, Deogaonkar M, Rezai A (2011) Intracranial air correlates with preoperative cerebral atrophy and stereotactic error during bilateral STN DBS surgery for Parkinson's disease. Stereotact Funct Neurosurg 89(4):246–252

Bilger A, Dequidt J, Duriez C, Cotin S (2011) Biomechanical simulation of electrode migration for deep brain stimulation. Med Comput Comput Assist Interv Miccai 2011 6891:339–346

Bilger A, Bardinet E, Fernandez-Vidal S, Duriez C, Jannin P, Cotin S (2014a) Intra-operative registration for stereotactic procedures driven by a combined biomechanical brain and CSF model. Lecture Notes in Computer Science, vol 8789, pp 76–85

Bilger A, Duriez C, Cotin S (2014b) Computation and visualization of risk assessment in deep brain stimulation planning. Stud Health Technol Inf 196:29–35

Cala LA, Thickbroom GW, Black JL, Collins DW, Mastaglia FL (1981) Brain density and cerebrospinal fluid space size: CT of normal volunteers. AJNR Am J Neuroradiol 2(1):41–47

Elias WJ, Fu KM, Frysinger RC (2007) Cortical and subcortical brain shift during stereotactic procedures. J Neurosurg 107(5):983–988

Hamze N, Bilger A, Duriez C, Cotin S, Essert C (2015) Anticipation of brain shift in deep brain stimulation automatic planning. Conf Proc IEEE Eng Med Biol Soc 2015:3635–3638

Hill DLG, Maurer CR, Maciunas RJ, Barwise JA, Fitzpatrick JM, Wang MY (1998) Measurement of intraoperative brain surface deformation under a craniotomy. Neurosurgery 43(3):514–526

Ivan ME, Yarlagadda J, Saxena AP, Martin AJ, Starr PA, Sootsman WK et al (2014) Brain shift during bur hole-based procedures using interventional MRI. J Neurosurg 121(1):149–160

Jackson RJ, Fuller GN, Abi-Said D, Lang FF, Gokaslan ZL, Shi WM et al (2001) Limitations of stereotactic biopsy in the initial management of gliomas. Neuro Oncol 3(3):193–200

Jin X, Lee JB, Leung LY, Zhang L, Yang KH, King AI (2006) Biomechanical response of the bovine pia-arachnoid complex to tensile loading at varying strain-rates. Stapp Car Crash J 50:637–649

Jin X, Ma C, Zhang L, Yang KH, King AI, Dong G et al (2007) Biomechanical response of the bovine pia-arachnoid complex to normal traction loading at varying strain rates. Stapp Car Crash J 51:115–126

Jin X, Yang KH, King AI (2011) Mechanical properties of bovine pia-arachnoid complex in shear. J Biomech 44(3):467–474

Jin X, Mao H, Yang KH, King AI (2014) Constitutive modeling of pia-arachnoid complex. Ann Biomed Eng 42(4):812–821

Kalia SK, Sankar T, Lozano AM (2013) Deep brain stimulation for Parkinson's disease and other movement disorders. Curr Opin Neurol 26(4):374–380

Levin E, Muravchick S, Gold MI (1981) Density of normal human cerebrospinal fluid and tetracaine solutions. Anesth Analg 60(11):814–817

Lewis O, Woolley M, Johnson D, Rosser A, Barua NU, Bienemann AS et al (2016) Chronic, intermittent convection-enhanced delivery devices. J Neurosci Methods 259:47–56

Maas SA, Ellis BJ, Ateshian GA, Weiss JA (2012) FEBio: finite elements for biomechanics. J Biomech Eng 134(1):011005

Mihai LA, Chin L, Janmey PA, Goriely A (2015) A comparison of hyperelastic constitutive models applicable to brain and fat tissues. J R Soc Interface 12(110):0486

Monea AG, Verpoest I, Vander Sloten J, Van der Perre G, Goffin J, Depreitere B (2012) Assessment of relative brain-skull motion in quasistatic circumstances by magnetic resonance imaging. J Neurotrauma 29(13):2305–2317

Schnaudigel S, Preul C, Ugur T, Mentzel HJ, Witte OW, Tittgemeyer M et al (2010) Positional brain deformation visualized with magnetic resonance morphometry. Neurosurgery 66(2):376–384 discussion 84

van Noort R, Black MM, Martin TR, Meanley S (1981) A study of the uniaxial mechanical properties of human dura mater preserved in glycerol. Biomaterials 2(1):41–45